

High energy factorization predictions for the charm structure function F_2^c at HERA

S. Munier and R. Peschanski

CEA, Service de Physique Théorique, CE-Saclay
F-91191 Gif-sur-Yvette Cedex, France

July 7, 2021

Abstract

High energy factorization predictions for F_2^c are derived using BFKL descriptions of the proton structure function F_2 at HERA. The model parameters are fixed by a fit of F_2 at small x . Two different approaches of the non perturbative proton input are shown to correspond to the factorization at the gluon or quark level, respectively. The predictions for F_2^c are in agreement with the data within the present error bars. However, the photon wave-function formulation (factorization at quark level) predicts significantly higher F_2^c than both gluon factorization and a next-leading order DGLAP model.

1 Motivation

High energy factorization [1, 2] is a QCD factorization scheme suited for high-energy hard processes - and in particular for deep-inelastic $e^\mp - p$ scattering in the small x -regime ($x \simeq \frac{Q^2}{W^2}$) (W^2 is the energy squared in the virtual photon-proton center of mass frame). This scheme takes into account the resummation of the $(\alpha_s \log \frac{1}{x})^n$ terms in the QCD perturbative expansion of the structure functions. It amounts to proving the factorization of the perturbative amplitude in terms of a gluon-gluon BFKL kernel [3] convoluted with a first order (virtual)photon-(virtual)gluon cross section. A graphical illustration of this property is given in figure 1. The main difference between this scheme and the renormalization group factorization [4] which is valid at finite x is that the former involves a bidimensional integration in transverse momentum k_\perp , whereas the latter is a convolution in energy. Interestingly enough, high energy factorization can be applied to the resummation of the $(\alpha_s \log \frac{W^2}{M^2})^n$ terms in heavy quark pair photoproduction, and the combined resummation for heavy quark lepto production involving $(\alpha_s \log \frac{W^2}{Q^2})^n$ and $(\alpha_s \log \frac{W^2}{M^2})^n$ terms can also be studied [1]. Our aim is to test the high energy factorization predictions for the massive charm quark pair contribution to F_2 at HERA.

In references [5, 6], a formulation and a phenomenological analysis of the proton structure function F_2 satisfying high energy factorization in the framework of Mueller's color dipole picture [7] of BFKL dynamics were proposed. F_2 is the triple transverse momentum convolution of a coefficient function, the BFKL kernel and a non perturbative term. The non perturbative inputs, which can be interpreted as the density and size of primary dipoles in the parton sea of the proton [6], lead to a satisfactory description of F_2 at HERA range, with 3 parameters. In this analysis, quarks were assumed massless, and the convolution integral was approximated by a steepest-descent method for sake of simplicity. However, since the coefficient functions were considered constant and the quarks massless, the procedure was not specifically a check of high energy factorization itself.

In the following, we shall discuss the high energy factorization predictions by taking full account of the convolution integral and of the massive quark component in the phenomenological analysis.

On the experimental point of view, the HERA experiments have recently

published [8] data for the contribution of charmed meson production to the structure function F_2 . Their analysis was based on D^0 and D^* meson tagging. This allows to single out the charm contribution F_2^c to the total structure function and thus to investigate the quark mass dependence of the structure functions. We use this nice possibility to check whether the high energy factorization scheme gives a correct prediction for the mass-dependent contribution both in x and Q^2 . Our analysis can be considered as the analog within the BFKL dynamics of the one which can be performed using ordinary renormalization group evolution [9, 10]. Thus, we are also aiming to see whether there are agreements or differences in charm lepto-production between the different schemes available for analyzing deep-inelastic scattering.

However, the high energy factorization scheme adapted to the proton structure functions is not uniquely defined in terms of the separation between perturbative and non-perturbative contributions. Indeed, an *a priori* different factorization exists in which the virtual photon is described in terms of a quark-antiquark wave function configuration which then interacts with the proton (see for instance [11, 12]). One of our goals is to investigate the possible differences between the two schemes. Recently also, some theoretical doubt has been cast on the validity of the operator product expansion in the low- x range due to the k_\perp -diffusion property [13] inherent to the BFKL dynamics. In the context of our structure function studies, we thus also want to discuss phenomenologically the kinematical range in x and Q^2 where high energy factorization is valid and not spoiled by k_\perp -diffusion in the low momentum region.

The plan of our study is the following. Section 2 recalls the formulation of high energy factorization for the pair production of quarks of mass M in terms of the coefficient functions and unintegrated gluon distribution in the proton. We give the M -dependent expression of the coefficient functions. In section 3, we derive the expression of the proton structure function including the charm component in the framework of high energy factorization. We derive a new constraint on the unintegrated gluon distribution function due to the renormalization group property at high k_\perp . In section 4, we consider the alternative model of factorization based on the wave function formulation. We show the connection between the two models. We prove the equivalence at perturbative level between both schemes for the hard vertex while they are based on different non-perturbative inputs. In section 5, both models are applied to a phenomenological fit of F_2 and parameter free predictions for

F_2^c , F_L , and F_L^c . The final section **6** contains our conclusions on the validity of the high energy factorization predictions at HERA and an outlook on future studies. Taking into account both present experimental and theoretical uncertainties, high energy factorization is proved to be in agreement with the present experimental data. However, more precise data could discriminate between the different schemes, since the photon wave function formulation predicts higher F_2^c than both the gluon factorization and a next-leading order DGLAP model.

2 High energy factorization

Let us compute the pair production of quarks of arbitrary mass M at the virtual photon vertex of deep-inelastic scattering (see figure 1). Using the high energy factorization scheme [1], the inclusive transverse (resp. longitudinal) structure functions F_T (F_L) can be expressed as follows:

$$F_{T,L}(Y, Q^2, M^2) = \frac{1}{4\pi^2\alpha_{em}} \frac{Q^2}{4M^2} \int d^2 k_\perp \int_0^\infty dy \times \hat{\sigma}_{\gamma^* g, T,L}(Y - y, q_\perp/M, k_\perp/M) \mathcal{F}(y, k_\perp), \quad (1)$$

where $Q^2 = -q^2$ is the virtuality of the photon. Y represents the rapidity range available for the reaction. $\mathcal{F}(y, k_\perp)$ is the unintegrated gluon distribution [1], which describes the probability of finding a gluon with a longitudinal momentum fraction $z = e^{-y}$ and two-dimensional transverse momentum k_\perp in the target. q_\perp is the photon transverse momentum in the photon-proton centre of mass frame. $\hat{\sigma}_{\gamma^* g, T,L}$ is the hard cross section for (virtual)photon-(virtual)gluon fusion computed at order $\alpha_s \alpha_{em}$.

In order to express more easily high energy factorization, it is convenient to work with triple Mellin-transforms with respect to the rapidity Y and transverse momenta k_\perp and q_\perp . The result is:

$$F_{T,L}(Y, Q^2, M^2) = \frac{1}{4\pi^2\alpha_{em}} \frac{Q^2}{4M^2} \int \frac{d\gamma'}{2i\pi\gamma'} \left(\frac{4M^2}{Q^2} \right)^{\gamma'} \int \frac{d\gamma}{2i\pi\gamma} \left(\frac{4M^2}{Q_f^2} \right)^\gamma \int \frac{dN}{2i\pi} e^{YN} h_{T,L,N}(\gamma', \gamma) \mathcal{F}_N(\gamma; Q_f^2), \quad (2)$$

where Q_f^2 stands for the factorization scale and the inverse Mellin-transforms in γ , γ' and N are given by complex integrals along the axes $\frac{1}{2} \pm i\infty$, $\frac{1}{2} \pm i\infty$

and $N_0 \pm i\infty$ (N_0 larger than the real part of the rightmost singularity in the N -plane) respectively. By definition, $h_{T,L,N}(\gamma', \gamma)$ is the triple inverse Mellin-transform of the hard γ^* -gluon cross-section, namely:

$$h_{T,L,N}(\gamma', \gamma) \equiv \gamma' \gamma \int \frac{d^2 q_\perp}{\pi q_\perp^2} \left(\frac{q_\perp^2}{4M^2} \right)^{\gamma'} \int \frac{d^2 k_\perp}{\pi k_\perp^2} \left(\frac{k_\perp^2}{4M^2} \right)^\gamma \times \int_0^\infty dY e^{-YN} \hat{\sigma}_{\gamma^* g, T, L}(Y, q_\perp/M, k_\perp/M) . \quad (3)$$

$\mathcal{F}_N(\gamma; Q_f^2)$ is obtained from the unintegrated gluon distribution $\mathcal{F}(y, k_\perp)$. It reads:

$$\mathcal{F}_N(\gamma; Q_f^2) \equiv \int_0^\infty dy e^{-yN} \int \frac{d^2 k_\perp}{\pi k_\perp^2} \left(\frac{k_\perp^2}{Q_f^2} \right)^{-\gamma} \mathcal{F}(y, k_\perp) . \quad (4)$$

Note that the coefficient functions $h_{T,L,N}$ are known to have a weak dependence on N [1], hence we will consider in the following only their values at $N = 0$ denoted $h_{T,L}(\gamma; M^2)$.

The final expression for the high energy factorized structure function is

$$F_{T,L}(Y, Q^2, M^2) = \int \frac{d\gamma}{2i\pi} \left(\frac{Q^2}{Q_f^2} \right)^\gamma h_{T,L}(\gamma; M^2) \frac{\mathcal{F}(Y, \gamma; Q_f^2)}{\gamma} , \quad (5)$$

where

$$\mathcal{F}(Y, \gamma; Q_f^2) = \int \frac{dN}{2i\pi} e^{YN} \mathcal{F}_N(\gamma; Q_f^2) \quad (6)$$

and the coefficient functions related to F_T and F_L respectively are [14]:

$$h_T(\gamma; M^2) = \frac{\alpha_s}{6\pi} \frac{4^{-\gamma}}{(1+2\gamma)(1-\frac{2}{3}\gamma)} \frac{\Gamma(1+\gamma)\Gamma^3(1-\gamma)}{\Gamma(2-2\gamma)} \frac{1}{1+\frac{4M^2}{Q^2}} \times \left\{ \left(\frac{4M^2}{Q^2} \right)^\gamma \left((3\gamma-1) + \frac{4M^2}{Q^2}(\gamma-2) \right) + \left(1 + \frac{4M^2}{Q^2} \right)^{\gamma-1} \times \left(2(1+\gamma)(2-\gamma) + \frac{4M^2}{Q^2}(7+\gamma-6\gamma^2 - \frac{4M^2}{Q^2}(\gamma-2)) \right) \times {}_2F_1 \left(1-\gamma, \frac{1}{2}; \frac{3}{2}; \frac{1}{1+\frac{4M^2}{Q^2}} \right) \right\} \quad (7)$$

and

$$\begin{aligned}
h_L(\gamma; M^2) = & \frac{\alpha_s}{6\pi} \frac{4^{-\gamma}}{(1+2\gamma)(1-\frac{2}{3}\gamma)} \frac{\Gamma(1+\gamma)\Gamma^3(1-\gamma)}{\Gamma(2-2\gamma)} \frac{1}{1+\frac{4M^2}{Q^2}} \times \\
& \left\{ \left(\frac{4M^2}{Q^2} \right)^\gamma \left(2(1-\gamma) + 3\frac{4M^2}{Q^2} \right) + \left(1 + \frac{4M^2}{Q^2} \right)^{\gamma-1} \times \right. \\
& \left. \left(4\gamma(1-\gamma) - \frac{4M^2}{Q^2} \left(3\frac{4M^2}{Q^2} + 4(1-\gamma) \right) \right) \times \right. \\
& \left. {}_2F_1 \left(1-\gamma, \frac{1}{2}; \frac{3}{2}; \frac{1}{1+\frac{4M^2}{Q^2}} \right) \right\}, \quad (8)
\end{aligned}$$

where ${}_2F_1(a, b; c; \zeta)$ is the hypergeometric function [15].

It is easy to check that in both limits $M^2 \rightarrow 0$ (light quarks [16]) and $Q^2 \rightarrow 0$ (heavy flavour photoproduction [1]), the well-known expressions for the coefficient functions are recovered.

Inserting the expressions (7,8) for $h_{T,L}(\gamma; M^2)$ and a model for $\mathcal{F}(Y, \gamma; Q_f^2)$ in formula (5), and summing over all active flavours weighted by their electric charges squared, we obtain the explicit expression for the proton structure functions.

3 The proton structure functions

Let us now introduce the QCD dipole model for the proton structure functions. This model satisfies high energy factorization and gives a phenomenological description of the unintegrated structure function $\mathcal{F}_N(\gamma; Q_f^2)$, see (4), in the framework of BFKL dynamics. We parametrize the factor

$$\frac{\mathcal{F}_N(\gamma; Q_f^2)}{\gamma} = \frac{\omega_N(\gamma; Q_f^2)}{N - \frac{\alpha_s N_c}{\pi} \chi(\gamma)}. \quad (9)$$

Notice the factor $1/\gamma$ which corresponds to the k_\perp integration in Mellin transform and thus, $\omega_N(\gamma; Q_f^2)$ appears as the residue of the BFKL pole in the integrated gluon distribution in the target. \mathcal{F}_N is assumed to contain the well-known BFKL singularity [3] at $N = \frac{\alpha_s N_c}{\pi} \chi(\gamma)$ with

$$\chi(\gamma) = 2\Psi(1) - \Psi(\gamma) - \Psi(1-\gamma). \quad (10)$$

The function $\omega_N(\gamma; Q_f^2)$ will explicitly depend on the nature of the target. It may also contain other singularities than the BFKL pole, which will be discussed later on. For a target of small size (parton, massive onium), it can be deduced from perturbative calculations, whereas for extended targets like a proton, it is supplied by a model.

Following the suggestion of ref. [6], one assumes for the proton structure functions the following scaling form:

$$\omega_{N \simeq 0}(\gamma; Q_f^2) = \omega(\gamma) \left(\frac{Q_f}{Q_0} \right)^{2\gamma}, \quad (11)$$

where $\omega(\gamma)$ and Q_0 are the non-perturbative inputs of the model. Indeed, the scaling assumption (11) is the simplest one allowing to obtain formulae independent of the arbitrary factorization scale Q_f (see equation (5)). Note that Q_0 can be considered to be independent of the quark mass M , which is quite a reasonable assumption for a non perturbative proton parameter. Inserting (9) and the expressions for the coefficient functions (7,8) in equation (5), and taking into account the scaling (11), the overall formula reads:

$$\begin{aligned} F_{T,L}(x, Q^2; Q_0^2) &= \sum_Q e_Q^2 F_{T,L}(Y_Q, Q^2, M_Q^2; Q_0^2) \\ &= \int \frac{d\gamma}{2i\pi} \left(\frac{Q^2}{Q_0^2} \right)^\gamma \omega(\gamma) \int \frac{dN}{2i\pi} \frac{\sum_Q e_Q^2 e^{Y_Q N} h_{T,L}(\gamma; M_Q^2)}{N - \frac{\alpha_s N_c}{\pi} \chi(\gamma)}, \end{aligned} \quad (12)$$

where

$$Y_Q = \log \frac{1}{x(1 + \frac{4M_Q^2}{Q^2})} \quad (13)$$

is the maximal available rapidity range for the produced gluons in association with quarks of mass M_Q . The summation \sum_Q takes into account the contributions of all active flavours with charge e_Q , mass M_Q .

The unintegrated gluon distribution in the proton $\mathcal{F}_N(\gamma; Q_f^2)$ is thus model dependent in particular through the input function $\omega(\gamma)$. However, let us show that it obeys a theoretical constraint when γ goes to infinity [17]. Indeed, as we shall demonstrate, this limit corresponds to a situation in which the intermediate gluon emitted from the dipole (see fig.1) has a large transverse momentum k_\perp . Hence its evolution from Q_0^2 up to k_\perp^2 is governed by the gluon-gluon DGLAP evolution equation (in its small- x approximation).

Let us then consider formula (4) and single out the integration region $k_\perp^2 \gg Q_0^2$. In this hard region where k_\perp -ordering of intermediate gluons is valid, the unintegrated gluon distribution is simply related to $\mathcal{G}(Y, k_\perp^2)$, the gluon distribution function in the proton at the scale k_\perp^2 , by:

$$\mathcal{F}(Y, k_\perp^2) = \frac{1}{\pi} \frac{d}{dk_\perp^2} \mathcal{G}(Y, k_\perp^2) . \quad (14)$$

Introducing the Mellin transform in rapidity, the gluon-gluon DGLAP evolution equation at small x (small N) reads

$$\int_0^\infty dY e^{-YN} \mathcal{G}(Y, k_\perp^2) \equiv \mathcal{G}_N(k_\perp^2) \simeq \left(\frac{k_\perp^2}{Q_0^2} \right)^{\frac{\alpha_s N_c}{\pi N}} \mathcal{G}_N(Q_0^2) . \quad (15)$$

Inserting formula (15) into equation (4) (for $k_\perp^2 \gg Q_0^2$), one gets a contribution

$$\mathcal{F}_N(\gamma; Q_f^2) \underset{|\gamma| \rightarrow \infty}{\simeq} \left(\frac{Q_f^2}{Q_0^2} \right)^{\frac{\alpha_s N_c}{\pi N}} \frac{1}{\gamma - \frac{\alpha_s N_c}{\pi N}} \mathcal{G}_N(Q_0^2) , \quad (16)$$

where $\gamma = \frac{\alpha_s N_c}{\pi N}$ is the well-known DGLAP singularity when N goes to 0.

As well-known, when γ is small $\chi(\gamma) \simeq 1/\gamma$ and the BFKL pole (9) can be approximated by

$$\frac{1}{N - \frac{\alpha_s N_c}{\pi} \chi(\gamma)} \underset{\gamma \rightarrow 0}{\simeq} \frac{1}{\gamma - \frac{\alpha_s N_c}{\pi N}} \frac{\gamma}{N} \quad (17)$$

and thus coincides with the DGLAP pole (16). However, in the large $|\gamma|$ region, $|\chi(\gamma)| \simeq 2 \log |\gamma|$ and thus the DGLAP pole at $\gamma = \frac{\alpha_s N_c}{\pi N}$ is separated from the BFKL singularity and dominates over it at small N .

Integrating over this dominant singularity in the inverse Mellin transform (6), we observe that the unintegrated structure function \mathcal{F} satisfies the constraint

$$\begin{aligned} \left| \left(\frac{Q_0^2}{Q_f^2} \right)^\gamma \frac{\mathcal{F}(\gamma, Y; Q_f^2)}{\gamma} \right| \underset{|\gamma| \rightarrow \infty}{\simeq} & \left| \frac{\alpha_s N_c}{\pi \gamma^3} e^{Y \frac{\alpha_s N_c}{\pi \gamma}} \mathcal{G}_{\frac{\alpha_s N_c}{\pi \gamma}}(Q_0^2) \right| \\ & \sim \frac{\alpha_s N_c}{\pi |\gamma|^3} \mathcal{G}_{N \simeq 0}(Q_0^2) \end{aligned} \quad (18)$$

assuming a regular input $\mathcal{G}_{N \simeq 0}(Q_0^2)$. On the other hand, the large $|\gamma|$ behaviour of the coefficient functions is given by

$$\begin{aligned} h_{T,L}(\gamma; M^2) \underset{\gamma \rightarrow \infty}{\simeq} & \frac{\Gamma(1+\gamma)\Gamma^3(1-\gamma)}{\Gamma(2-2\gamma)} {}_2F_1(1-\gamma, 1/2; 3/2; 1) \times \\ & \times \left\{ \text{terms of the form } \gamma^\alpha \left(\frac{4M^2}{Q^2} \right)^\beta \right\} \\ & \sim e^{-\pi|\gamma|} \times \{\text{Power-like terms}\} , \end{aligned} \quad (19)$$

and thus gives an exponential cutoff at $\gamma \simeq \frac{1}{\pi}$.

The following remarks are in order:

- The obtained behaviour (16) for $\mathcal{F}_N(\gamma; Q_f^2)$ at $|\gamma|$ large is in agreement with the scaling assumption (11) at the pole $\gamma = \frac{\alpha_s N_c}{\pi N}$.
- Most importantly, the large $|\gamma|$ behaviour of the coefficient functions $|h_{T,L}(\gamma, M^2)| \simeq e^{-\pi|\gamma|}$ dominates over the unintegrated structure function $\mathcal{F}(Y, \gamma; Q_f^2)$ which is only power-like in γ , showing that the main integration region is for finite $|\gamma| \leq \frac{1}{\pi}$.
- The large $|\gamma|$ behaviour of $\mathcal{F}(Y, \gamma; Q_f^2)$ is actually not dominated by the BFKL singularity but by the DGLAP singularity which differ in this domain. However, we shall neglect this modification occurring in a domain where the integrand is cutoff by the coefficient functions. A more detailed analysis of high energy factorization could need taking care of this modification.

4 High energy factorization at the quark level

In the previous section, we have found that the main integration region is for finite $|\gamma|$. In fact, the structure of the integrand singularity at $\gamma = 0$ appears to be essential both for the theoretical analysis and the phenomenological application. We note that in formulae (7) and (8) for the coefficient functions, ${}_2F_1(1-\gamma, \frac{1}{2}; \frac{3}{2}; 1/(1+4M^2/Q^2)) \propto 1/\gamma$ when γ goes to 0. We thus find that the Mellin-transform $h_{T,L,N}(\gamma; M^2)/\gamma$ of $\hat{\sigma}$ in formula (1) has in general a double pole at $\gamma = 0$ (but for e.g. h_L when $M^2 = 0$). It is easy to realize that this double pole corresponds to an extra $(\log k_\perp^2/Q^2)$ in the small k_\perp -behaviour

of the hard photon-gluon cross section due to the quark propagator (see fig.1). This behaviour is thus characteristic of the high energy factorization formalism at the perturbative level.

However, it is well-known [18] that there is an ambiguity in the separation between perturbative and non perturbative contributions in the small- k_\perp domain. The relevance of the perturbative double pole depends on the physical picture of the non perturbative input. For definiteness, we will consider two classes of models relying on different hypotheses on the behaviour of the residue function $\omega(\gamma)$ near $\gamma = 0$. In the first type of models, with

$$\omega(\gamma) \underset{\gamma \rightarrow 0}{\simeq} (\text{constant}) , \quad (20)$$

one keeps the full perturbative information on the γ^* -gluon vertex. This corresponds to the *factorization at the gluon level* (see fig.1). In the second class of models, the perturbative singularity at the hard vertex is smoothed by the proton scaling function (11), namely

$$\omega(\gamma) \underset{\gamma \rightarrow 0}{\simeq} (\text{constant}) \times \gamma . \quad (21)$$

The resulting single pole at the hard vertex may be interpreted as a direct pointlike coupling of the virtual photon to the quark. This may be interpreted as a *factorization at the quark level* (see fig.1).

In summary, either the contribution of the off-shell gluon at the hard vertex is maintained, or it is compensated by the non perturbative input. In the first case (model 1), the hard photon is assumed to probe the gluon content of the target, and consequently, the $1/\gamma^2$ singularity of the coefficient functions is preserved. In the latter case (model 2), the photon probes the quark distribution and thus the coefficient function double pole can be compensated by the proton scaling function $\omega(\gamma) \propto \gamma$ when γ goes to 0, see formula (12).

As we shall see, a prototype of model 2 is provided by the wave function formulation of the photon-proton interaction [11, 12]. In this framework, deep-inelastic scattering processes are formulated in terms of the probability distribution of a $Q\bar{Q}$ pair (considered as a dipole configuration) in the virtual photon, convoluted by the dipole-proton cross section. In our case, the dipole-proton cross-section is described by the convolution of the probability distribution of primordial dipoles in the proton times the dipole-dipole BFKL

cross-section [7]. This will allow a direct comparison between model 1 and 2, which have a similar parametrization differing only by the pole structure at $\gamma = 0$.

In references [11, 12], one finds the expressions for the wave function and probability distribution of the photon $Q\bar{Q}$ states. The virtual photon can be described in terms of probability distributions (when the interference terms [19] are not relevant) depending on the quark mass M and charge e

$$\begin{aligned}\Phi_T^\gamma(z, r; Q^2, M^2) &= \frac{\alpha_{em} N_c}{2\pi^2} e^2 \left((z^2 + (1-z)^2) \epsilon^2 K_1^2(\epsilon r) + M^2 K_0^2(\epsilon r) \right) , \\ \Phi_L^\gamma(z, r; Q^2, M^2) &= \frac{\alpha_{em} N_c}{2\pi^2} 4e^2 Q^2 z^2 (1-z)^2 K_0^2(\epsilon r) ,\end{aligned}\quad (22)$$

where $\epsilon^2 = z(1-z)Q^2 + M^2$, and the $K_{0,1}$ are the Bessel functions of second kind [15]. $\Phi_{T,L}^\gamma(z, r; Q^2, M^2)$ are the probability distributions of finding a dipole configuration of transverse size r at a given z , the variable z (resp. $(1-z)$) being the photon light-cone momentum fraction carried by the antiquark (resp. quark).

The transverse and longitudinal total cross sections $\sigma_{T,L}$ read

$$\sigma_{T,L} = \int d^2 r dz \Phi_{T,L}^\gamma(r, z; Q^2, M^2) \int d^2 r_p dz_p \Phi^p(r_p, z_p) \sigma_d(r, r_p; Y) , \quad (23)$$

where we have introduced the probability distributions $\Phi^p(r_p, z_p)$ of dipoles inside the proton [5, 6, 20]. The dipole-dipole cross section $\sigma_d(r, r_p; Y)$ is assumed not to depend on z . This hypothesis means that we neglect sub-asymptotic effects related to the momentum carried by the quarks (while we do not neglect the quark masses). In practice, it corresponds to consider $N \simeq 0$ in the Mellin-transform with respect to rapidity as in section 2.

$\sigma_d(r, r_p; Y)$ reads [7, 20, 21]:

$$\sigma_d(r, r_p; Y) = 4\pi r r_p \int \frac{d\gamma}{2i\pi} \left(\frac{r_p}{r} \right)^{2\gamma-1} e^{\frac{\alpha_s N_c}{\pi} \chi(\gamma) Y} A_{el}(\gamma) , \quad (24)$$

where $\chi(\gamma)$ is the BFKL kernel (10) and the elementary two-gluon exchange amplitude is given by

$$A_{el}(\gamma) = \frac{\alpha_s^2}{16\gamma^2(1-\gamma)^2} . \quad (25)$$

We define the non-perturbative scale Q_0 characterizing the average dipole size by [20]

$$\int d^2r_p r_p^{2\gamma} \int dz_p \Phi^p(r_p, z_p) \equiv \frac{n_{eff}(\gamma)}{(Q_0^2)^\gamma} , \quad (26)$$

where n_{eff} can be interpreted as the γ -dependent average number of primary dipoles in the proton. Finally, the Mellin-transform of the photon wavefunction is defined by:

$$\int \frac{d^2r}{2\pi} (r^2)^{1-\gamma} \int dz \Phi_{T,L}^\gamma(r, z; M^2) = \phi_{T,L}(\gamma; M^2) (Q^2)^{\gamma-1} , \quad (27)$$

where we have explicitly factorized the photon scale dependence. After plugging these formulae into equation (23), and performing the integrations with respect to r , r_p and z , z_p one finds:

$$\sigma_{T,L} = \frac{32\pi^2}{Q^2} \int \frac{d\gamma}{2i\pi} \left(\frac{Q^2}{Q_0^2} \right)^\gamma e^{\frac{\alpha_s N_c}{\pi} \chi(\gamma) Y} \phi_{T,L}(\gamma; M^2) A_{el}(\gamma) n_{eff}(\gamma) . \quad (28)$$

Inserting the virtual photon probability distribution $\Phi_{T,L}^\gamma(r, z; Q^2, M^2)$ into equation (27) and after a straightforward but tedious calculation, one finds expressions for $\Phi_{T,L}(\gamma; M^2)$ which can be cast into the following form:

$$\phi_{T,L}(\gamma; M^2) = \frac{\alpha_{em} e^2}{\alpha_s} \frac{N_c}{4\pi} \frac{h_{T,L}(\gamma; M^2)}{\gamma} \left\{ 2^{-2\gamma+3} (1-\gamma)^2 \frac{\Gamma(1-\gamma)}{\Gamma(\gamma)} \right\} , \quad (29)$$

where $h_{T,L}(\gamma; M^2)/\gamma$ is related to the Mellin transform of $\hat{\sigma}$ accounted for in the preceding section (see equation (3)). It is clear from formula (29) that the double pole of $h_{T,L}(\gamma; M^2)/\gamma$ is turned into a single pole due to the factor $\{...\}$. This shows that the factorization of the probability distributions $\phi_{T,L}(\gamma; M^2)$ at the hard vertex leads to the singularity structure (21) of model 2.

Some comments are in order:

- The γ -dependent but M^2 -independent factor $\{...\}$ is nothing but the coupling of the virtual gluon to the $Q\bar{Q}$ pair configuration of the virtual photon wave function. Indeed, the two-gluon exchange elementary

amplitude (25) can be rewritten as

$$A_{el}(\gamma) = \frac{\alpha_s^2}{16\gamma^2(1-\gamma)^2} = \alpha_s^2 v(\gamma) v(1-\gamma) , \quad (30)$$

with

$$v(\gamma) = \frac{2^{-2\gamma-1}}{\gamma} \frac{\Gamma(1-\gamma)}{\Gamma(1+\gamma)} \quad (31)$$

which is, up to a factor $\frac{\alpha_s N_c}{\pi}$, the eikonal coupling of a gluon to a dipole [6, 22] at the lower vertex. Thus, the factorized factor $\{\dots\}$ is nothing else than $v(1-\gamma)$, i.e. the coupling of the gluon to the photon's dipole configuration, as shown in figure 1.

- Using (30,31), equation (29) can be rewritten

$$A_{el}(\gamma) \cdot \phi_{T,L}(\gamma; M^2) = \alpha_{em} \frac{\alpha_s N_c}{4\pi} v(\gamma) \cdot \frac{h_{T,L}(\gamma; M^2)}{\gamma} . \quad (32)$$

In the hard perturbative domain where we consider a photon-dipole interaction with a dipole of small size, formula (32) means that both high energy factorization and the wave-function formalism are identical. The cross section can be equivalently factorized in two ways: either by the convolution of the photon gluon cross section times the gluon coupling to the dipole (right hand side), or by the probability distribution of a pair of quarks in the photon times the dipole-dipole elementary interaction (left hand side).

However, as previously discussed, the non perturbative input may lead to distinguishable models.

- At the level of the non perturbative input, we note a relation between the two formulations (12) and (23), namely

$$\omega(\gamma) = \frac{2\alpha_s N_c}{\pi} n_{eff}(\gamma) \frac{v(\gamma)}{\gamma} , \quad (33)$$

which generalizes the result for $M = 0$, obtained in ref. [6].

5 Phenomenology

Following our theoretical discussions of the previous sections, we will consider two definite models relying on different formulations of the residue function $\omega(\gamma)$. On the one hand, the model 1, with

$$\omega(\gamma) = C_1 \text{ (constant)} \quad (34)$$

corresponds to the factorization at the gluon level (see figure 1). On the other hand, in the wave function formulation of the dipole model of section 4, we can reformulate the integrand of the structure function (see equation (12)) by using relation (32), namely:

$$\frac{h_{T,L}(\gamma)}{\gamma} \cdot \omega(\gamma) = \left(\frac{4\pi\alpha_s}{\alpha_{em}N_c} \right) \phi(\gamma) \cdot \omega(\gamma) \cdot v(1-\gamma) . \quad (35)$$

In the model 2, the hard vertex is thus described by factorizing $\phi(\gamma)$ which means that we consider

$$\omega(\gamma) \cdot v(1-\gamma) = C_2 \text{ (constant)} . \quad (36)$$

As expected, $\omega(\gamma)$ behaves like γ when γ goes to zero in this framework. In the large $|\gamma|$ region ($\gamma = 1/2 + i\nu$, ν goes to infinity), one has $|\omega(\gamma)| \simeq |C_2/v(1-\gamma)| \propto |\gamma|^2$. The exponential cutoff of $\phi_{T,L}$ is the same as the one (19) of the coefficient function and thus the large $|\gamma|$ constraint is satisfied. Note that, in both cases, the proton structure functions depend on three free parameters only: the global normalization C_1 or C_2 , the effective constant strong coupling α_s , and the non perturbative scale Q_0 .

We determine these parameters for the two models by a fit of $F_2 = F_T + F_L$ in their kinematical region of validity ($x \leq 10^{-2}$). In this region, Q^2 is automatically limited by the HERA kinematics. Using the corresponding 103 experimental points given by the H1 collaboration [23], we fit our results with the contribution of the three light quarks u, d, s (assumed massless) and of the charm quark (mass M_c). As usual, we will vary M_c in the range $1.35 - 1.7$ GeV [8].

The F_2 -fit for the medium mass $M_c = 1.5$ GeV is displayed in figure 2, together with the predictions for its charm component F_2^c . In table I, we give the χ^2 and the value of the fit parameters for the fits for model 1 and 2 and

for $M_c = 1.35, 1.5$, and 1.7 . For model 1, the χ^2 per point is always less than 0.9, while for model 2 it is even lower.

Some comments on the parameter values are in order. For fit 1, the value of Q_0 is around 330 MeV which is a typical non perturbative scale for the proton. The value of the effective coupling constant in the BFKL mechanism α_s (0.07) is rather low. This value would amount to an effective pomeron intercept $\alpha_P = 1 + \alpha_s N_c 4 \log 2/\pi \simeq 1.18$. (It is known that α_P is influenced by sub-leading corrections to the BFKL kernel, see e.g. references [24]). Note that the fit of model 1 for F_2 in the framework of the QCD dipole model and high energy factorization is compatible with the previous ones in the same framework [6].

We also in parallel performed the phenomenological analysis using the model 2-ansatz (36). The obtained fit reproduces fairly well the data for F_2 (see figure 2). As indicated by the lower value of χ^2 , it seems that the data, especially in the small- x small- Q^2 region are even better reproduced than for model 1. Note that the value of $Q_0 \simeq 1.2$ is substantially higher and the effective coupling constant α_s is larger ($\simeq \alpha_s(M_Z)$).

Following the factorization scheme and using formulae (5) (model 1) or (23) (model 2), we obtain now parameter-free predictions for the longitudinal structure functions F_L and F_L^c (see figure 3). The predictions for F_L and F_L^c are shown together with the indirect H1 determination of F_L [25]. As expected, F_L^c becomes a significant part of F_L at small x and high Q^2 . As already noticed [6], the predictions are low but compatible with the present large error bars. Note also that the determination [25] depends on the theoretical scheme one considers [26], so it is difficult to draw any conclusion on F_L at this stage.

The main outcome of our analysis is a parameter free prediction for F_2^c , the charm component of the structure function (see fig.4). When compared to ZEUS and H1 data for the charm component in the same range in x and Q^2 [8], we find a good agreement within the present experimental error bars. The extrapolation of the prediction to the kinematical range of EMC data is correct while the dipole model is not expected to be valid in this region.

Looking in more detail to the predictions of model 1 (figure 4-a) and model 2 (figure 4-b), we observe the following features. The dispersion of the results with respect to M_c is rather small for fit 1 with a maximum of 10% when x reaches 10^{-4} . Moreover, the prediction is comparable to the next-leading order GRV prediction which proves that F_2^c cannot allow one to

distinguish between the two approaches.

For model 2, the predictions obtained for F_2^c are displayed in figure 4-b. The prediction for the HERA region is quite satisfactory and, interestingly enough, somewhat higher than both the NLO GRV predictions and fit 1. It would certainly be useful to deserve some experimental and theoretical attention to this difference. Indeed, the scheme of model 2 which is based on a different factorization than both GRV and model 1 could lead to a better understanding of the data. A sensible decrease of the experimental errors on F_2^c in the region where Q^2 is moderate (of the order 10 GeV 2) and x small (of the order 10 $^{-3}$) could allow a refinement of this analysis.

All in all, the comparison of fits 1 and 2 shows that the high energy factorization prediction for F_2^c depends on the non-perturbative input in the HERA range. Indeed, a different factorization scheme such as model 2 corresponds to a modification of the non perturbative input of high energy factorization. However, the largest uncertainty due to this effect is of the order 20% and less than the experimental uncertainty. Thus, there is no present evidence of a distinction between these schemes and the DGLAP scheme.

6 Conclusions and outlook.

Let us summarize the results of our analysis.

- (i) High energy factorization [1] gives predictions for the x and Q^2 behaviour of F_2^c at low x in the framework of models based on the BFKL dynamics. The charm prediction is fixed by high energy factorization once the total proton structure function F_2 is fit. More generally, this prediction is well defined for any quark mass.
- (ii) The factorization of the hard virtual photon vertex at the level of the exchanged gluon (model 1) or the exchanged quark (model 2) leads to two specific classes of models which both give a satisfactory fit of F_2 . The formulation [11, 12] based on the virtual photon wave function is shown to lead to a physical realization of model 2.
- (iii) Both models lead to predictions for F_2^c in agreement with the present data. However, the second scheme leads to a higher F_2^c than both model 1 and NLO DGLAP predictions [8]. This justifies further experimental and theoretical studies.

(iv) The derivation leads to a new constraint on the unintegrated gluon distribution in the proton due to the renormalization group evolution at high transverse momentum of the off-shell gluon.

It is interesting to discuss the gluon distribution functions in this framework. In the high energy factorization scheme, it would consist in an expression like (12), replacing the coefficient functions by unity. However, the convergence of the integral (12) is then not *a priori* preserved and even if convergent, the dependence of the result on the large $|\gamma|$ region would be larger, casting a doubt on the relevance of the BFKL dynamics. In the wavefunction framework, the extraction of the gluon structure function is even more problematic since the factorization is at the quark level (see fig.1). On a more general ground, this confirms the statement of caution [14] about extracting the gluon from this kind of analysis, especially at low x . We think that this point deserves more studies.

Finally, the running of the coupling constant and other aspects of next leading order BFKL resummation features have been neglected in the present analysis. The small value obtained for the effective coupling constant in the fits clearly indicates that such effects are important and should be included in a more detailed analysis. Indeed, a preliminary theoretical hint on the effective behaviour of the pomeron singularity at NLO accuracy leads to a small and constant intercept of the order 0.2 [24]. A NLO BFKL analysis of F_2^c would thus be required in view of a future improvement of the experimental analysis.

Acknowledgments

We thank Stefano Catani for fruitful discussions and Henri Navelet and Christophe Royon for stimulating remarks.

References

- [1] S. Catani, M. Ciafaloni, F. Hautmann, *Nucl. Phys.* **B366** (1991) 135.
- [2] J. C. Collins, R. K. Ellis, *Nucl. Phys.* **B360** (1991) 3.
E. M. Levin, M. G. Ryskin, Yu. M. Shabelskii, A. G. Shuvaev, *Sov. J. Nucl. Phys.* **53** (1991) 657.
- [3] V. S. Fadin, E.A. Kuraev and L.N. Lipatov, *Phys. Lett.* **B60** (1975) 50;
I. I. Balitsky and L.N. Lipatov, *Sov. J. Nucl. Phys.* **28** (1978) 822.
- [4] See for instance J.C. Collins, D.E. Soper, G. Sterman, *in* Perturbative quantum chromodynamics, ed. A.H. Mueller (*World Scientific*, Singapore, 1989).
- [5] H. Navelet, R. Peschanski, Ch. Royon, *Phys. Lett.* **B366** (1995) 329.
- [6] H. Navelet, R. Peschanski, Ch. Royon, S. Wallon, *Phys. Lett.* **B385** (1996) 357.
- [7] A. H. Mueller, *Nucl. Phys.* **B415** (1994) 373.
A. H. Mueller, B. Patel, *Nucl. Phys.* **B425** (1994) 471.
A. H. Mueller, *Nucl. Phys.* **B437** (1995) 107.
- [8] H1 Coll., C. Adloff et al., *Z. Phys.* **C72** (1996) 593;
ZEUS Coll., J. Breitweg et al., *Phys. Lett.* **B407** (1997) 402.
- [9] M. Glück, E. Reya and A. Vogt, *Z. Phys.* **C67** (1995) 27.
- [10] R. S. Thorne and R.G. Roberts, [hep-ph/9709442](#), [hep-ph/9711223](#) and references therein.
- [11] J. D. Bjorken, J. B. Kogut, D. E. Soper, *Phys. Rev* **D3** (1971) 1382.
- [12] N. N. Nikolaev, B. G. Zakharov, *Phys. Lett.* **B332** (1994) 184.
- [13] A. H. Mueller, *Phys. Lett.* **B396** (1997) 251.
- [14] S. Catani, *Z. Phys.* **C75** (1997) 665.
- [15] P.S. Gradshteyn, I.M. Ryzhik, Table of integrals series and products, (*Academic Press*, New York and London, 1965).

- [16] S. Catani, F. Hautmann, *Nucl. Phys.* **B427** (1994) 475-524.
- [17] We thank S. Catani for suggesting to us these remarks.
- [18] S. Catani, *Z. Phys.* **C70** (1996) 263.
- [19] A. Bialas, R. Peschanski, *Phys. Lett.* **B387** (1996) 405.
- [20] A. Bialas, *Acta Phys. Pol.* **B28** (1997) 1239.
- [21] R. Peschanski, unpublished.
- [22] S. Wallon, *Thèse de doctorat*, Orsay, 1996.
- [23] H1 Coll., T. Ahmed et al., *Phys. Lett.* **B348** (1995) 681;
ZEUS Coll., M. Derrick et al., *Z. Phys.* **C68** (1995) 569.
- [24] M. Ciafaloni, [hep-ph/9709390](#) and references therein.
- [25] H1 Coll., C. Adloff et al., *Phys. Lett.* **B393** (1997) 452.
- [26] R. S. Thorne, *Phys. Lett.* **B392** (1997) 463,
[hep-ph/9701241](#), [/9708302](#), [/9710541](#).

TABLE CAPTION

Table I

Total proton structure function: χ^2 and parameters for the fits

For each model, we give the χ^2 value for 103 points and the parameters C , Q_0 and α_s . Three different charm masses, $M_c = 1.35, 1.5, 1.7$ GeV are considered. **I-a.** Model 1. **I-b.** Model 2.

M_c	χ^2	C_1	Q_0	α_s
1.35	77	19.88	0.334	0.070
1.50	82	20.27	0.326	0.070
1.70	88	20.70	0.321	0.070

a. Model 1

M_c	χ^2	C_2	Q_0	α_s
1.35	51	8.68	1.208	0.105
1.50	51	9.22	1.215	0.104
1.70	52	9.86	1.227	0.103

b. Model 2

Table I

FIGURE CAPTIONS

Figure 1 *Quark-antiquark pair lepto production at high energy*

The upper vertex represents the virtual photon (with momentum q)-virtual gluon (with momentum k) fusion diagram through the production of a pair of quarks of mass M . The proton (with momentum p) interacts with the gluon through the BFKL kernel. The non perturbative proton vertex is schematized by the shaded area. Model 1 corresponds to factorization at the gluon level, model 2 at the quark level, see text.

Figure 2 *The fits (model 1 and model 2) for the structure function F_2*

The structure function F_2 and its parametrization are displayed for model 1 and model 2. The fits have been performed with the 1994 H1 data (triangles) but only using the 103 experimental points for which $x \leq 10^{-2}$. Continuous line: fit for model 1; dashed line: fit for model 2; dotted line: prediction for the charm component F_2^c , for $M_c = 1.5$ GeV and model 1. The available H1 data are marked by stars.

Figure 3 *Predictions for the longitudinal structure functions F_L (continuous line) and F_L^c (dashed line)*

Continuous line: model 1; dashed line: model 2; dotted line: F_L^c (model 1). The experimental points available from H1 [25] have been reported on the graph.

Figure 4 *Predictions for F_2^c*

The reported data on the plots are from H1 D^0 (squares), H1 D^* (circles), ZEUS D^* (full circles), and at lower energy, EMC data (crosses). The predictions of our models are displayed by a band delimited by the two continuous lines ($M_c = 1.35$ for the higher curves and $M_c = 1.7$ for the lower curves). Extrapolations of our predictions down to the EMC range are plotted as dot-dashed lines.

Figure 4-a: model 1 predictions. The GRV prediction [9] based on NLO

analytic calculation is indicated by the shaded band (borrowed from ref. [8], second paper).

Figure 4-b: model 2 predictions: the band of solutions is delimited by thick lines. The model 1 predictions are recalled by the band delimited by thin lines, for comparison.

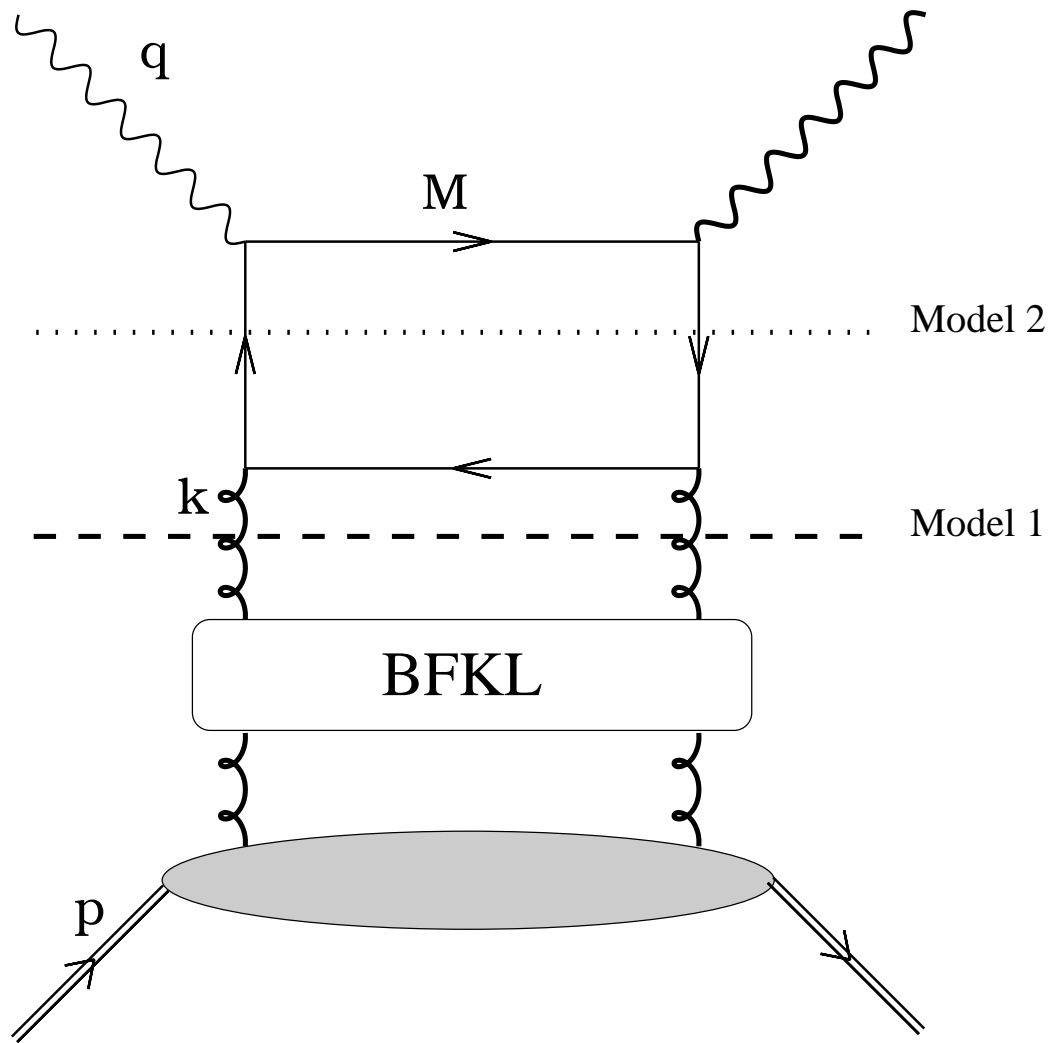


Figure 1

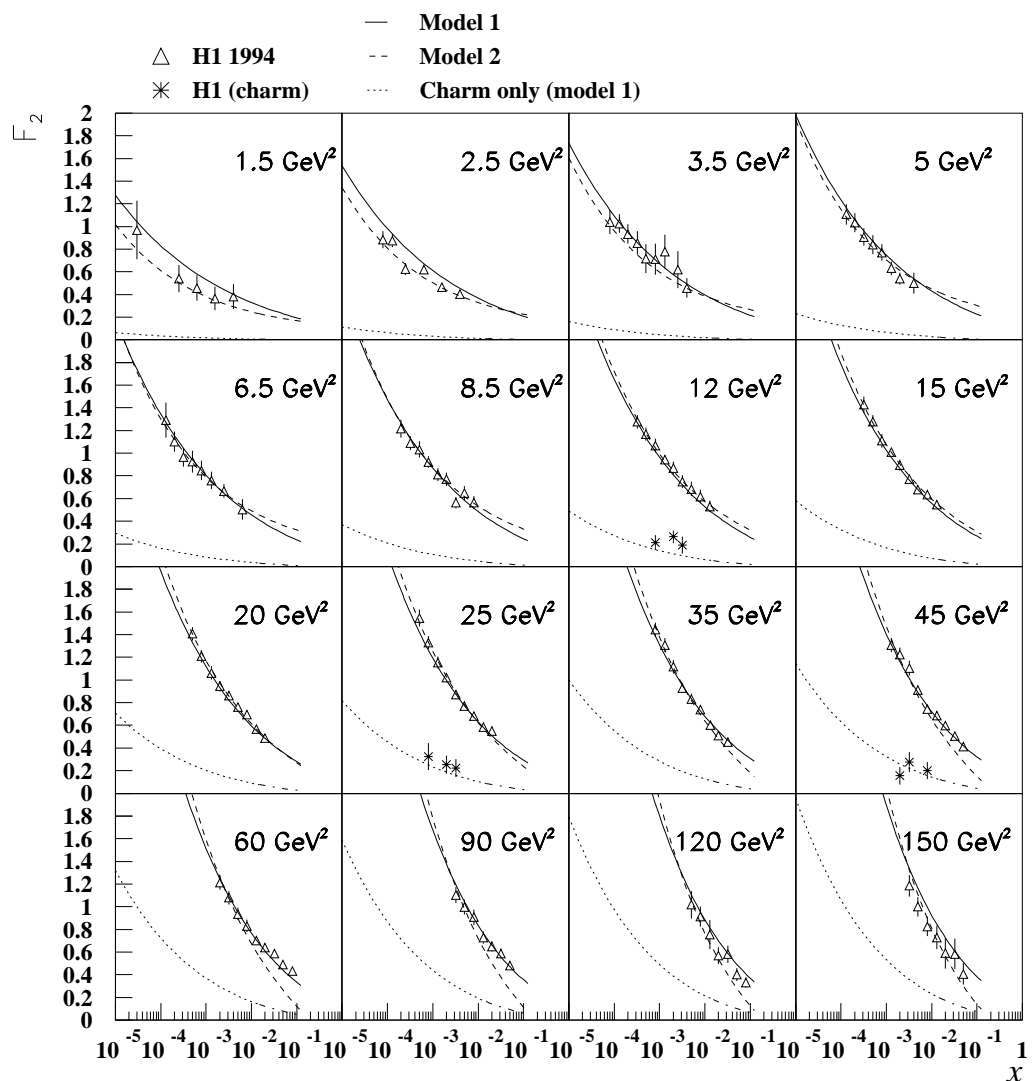


Figure 2

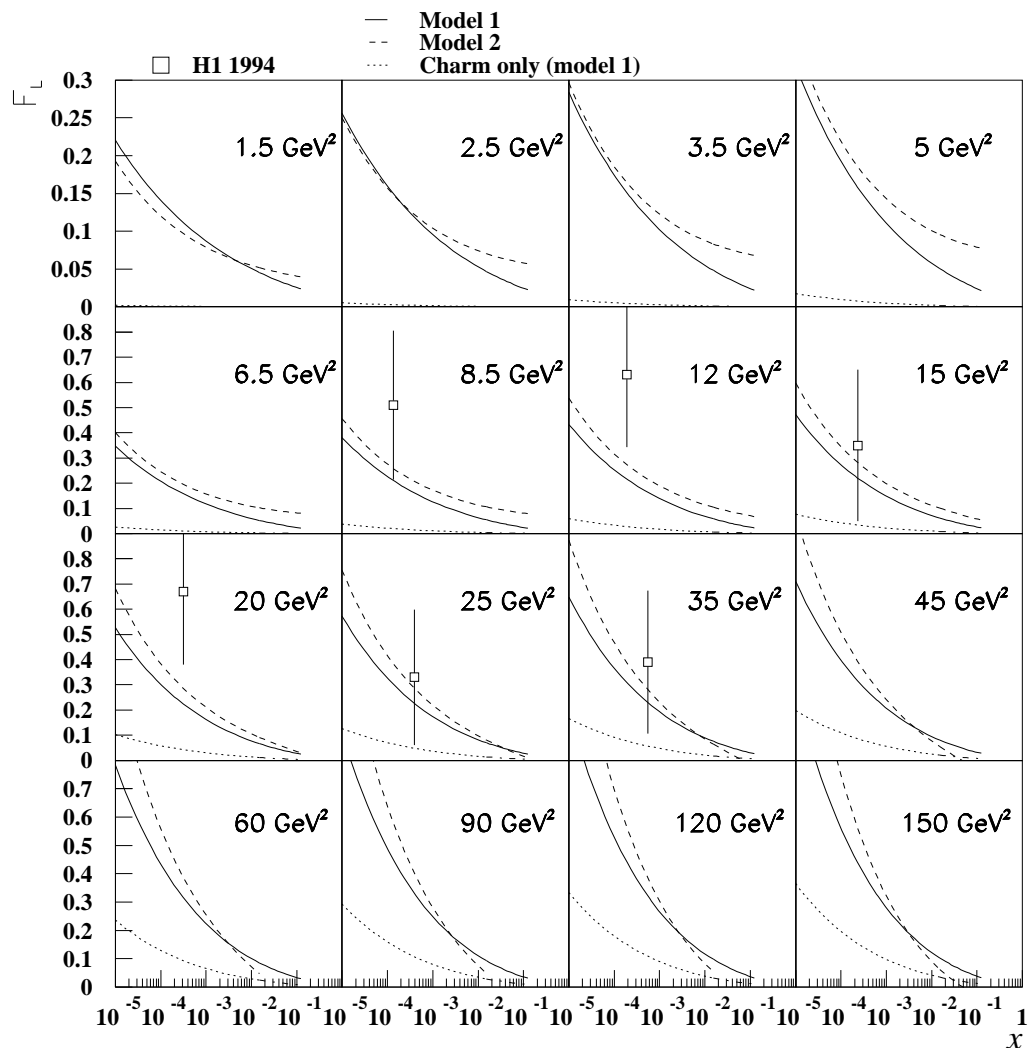


Figure 3

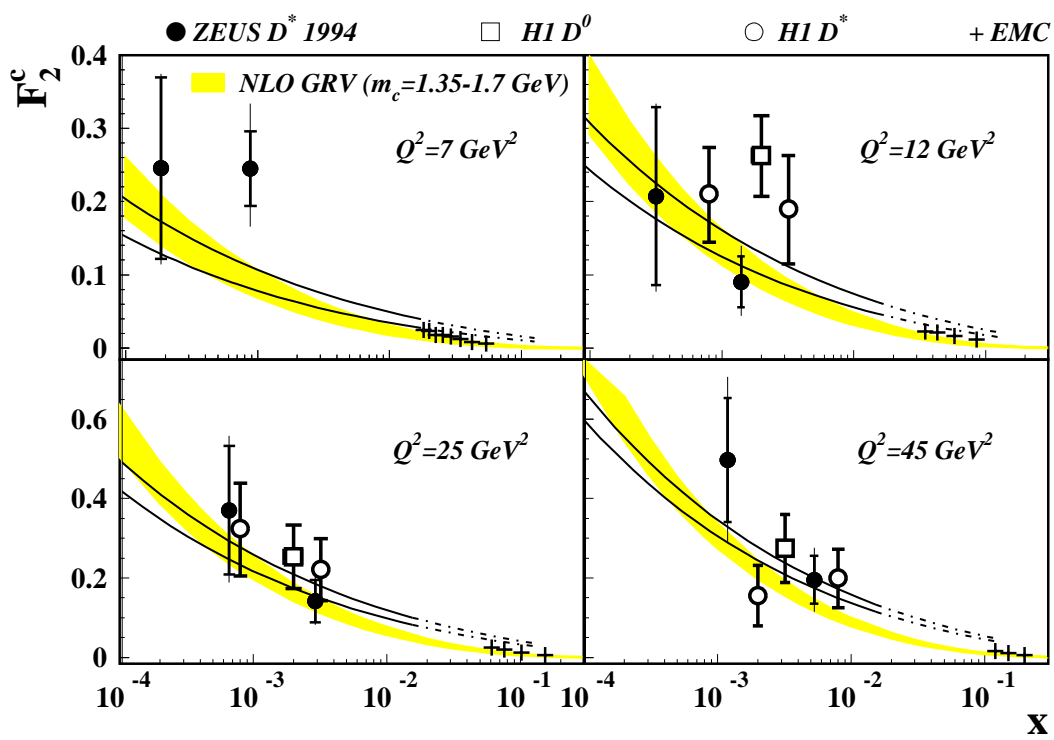


Figure 4-a

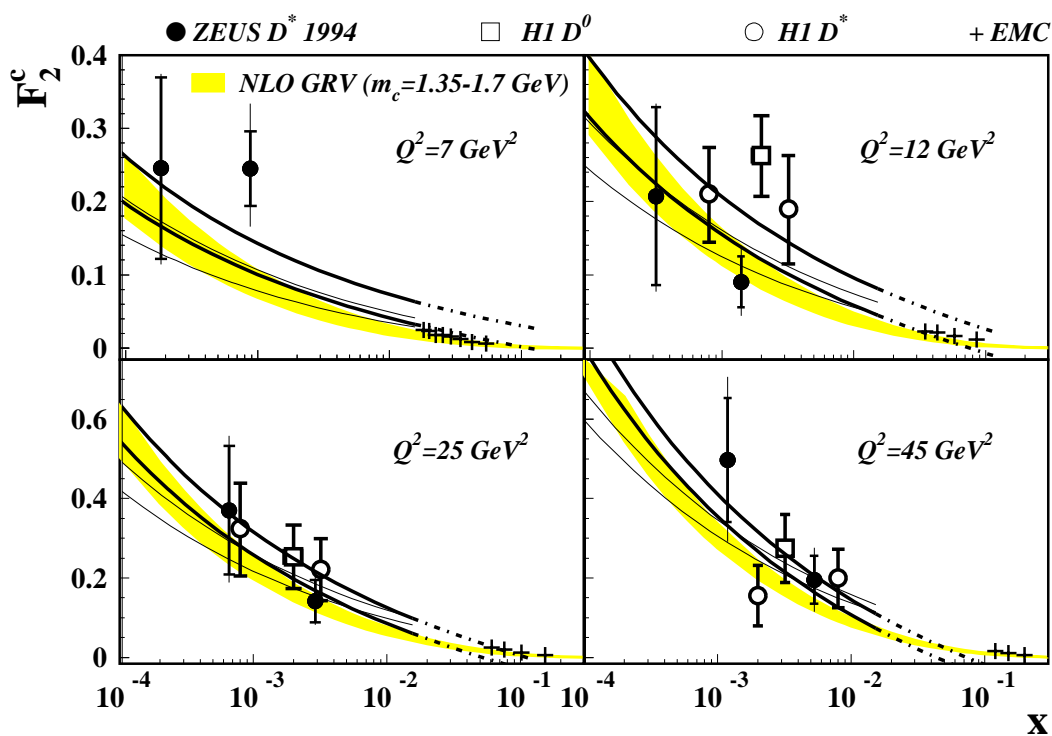


Figure 4-b